Phonon thermal properties of graphene from molecular dynamics using different potentials

Ji-Hang Zou (邹济杭), Zhen-Qiang Ye (叶振强), and Bing-Yang Cao (曹炳阳)[a)]
Key Laboratory for Thermal Science and Power Engineering of Ministry of Education, Department of Engineering Mechanics, Tsinghua University, Beijing 100084, China

(Received 21 July 2016; accepted 20 September 2016; published online 6 October 2016)

Phonon thermal transport in graphene has attracted significant interest in recent years. Phonon thermal properties of graphene are investigated by molecular dynamics simulations using the Tersoff, Tersoff-2010, REBO, and AIREBO potentials. By calculating the phonon properties and thermal conductivity of graphene, the performance of the potentials is evaluated based on comparisons with experimental data. It shows that the Tersoff-2010 and REBO display better dispersion curves for graphene than the original Tersoff and AIREBO. The Tersoff-2010 correctly provides the Γ point phonon velocities of the LA and TA branches as well as the G peak frequency with a value of 46 THz. In addition, the acoustic phonon relaxation time derived from the Tersoff-2010 satisfies the ideal relation "$\tau^{-1} \propto \nu^2$." It is also found that the Tersoff-2010 provides the highest graphene thermal conductivity among the used potentials, and estimates about 30.0% contribution for flexural phonons to the total thermal conductivity. By comparison, the Tersoff-2010 potential is demonstrated to be the most suitable one to describe the phonon thermal properties of graphene. *Published by AIP Publishing.* [http://dx.doi.org/10.1063/1.4963918]

I. INTRODUCTION

Graphene, a two-dimensional material formed of hexagonally arranged carbon atoms, has attracted significant attention in the thermal management field of electronic and optic nanodevices due to its ultrahigh thermal conductivity of 1000-5000 W/(m K).[1–7] Research has demonstrated that graphene is a prospective candidate for thermal management applications, such as heat spreaders, thermal interface materials, and nanocomposites, owing to its extraordinary thermal properties.[8–11] Seol *et al.*[12] discovered that the thermal conductivity of supported graphene is superior to most metals despite phonon-substrate scattering. Lee *et al.*[13] and Cepellotti *et al.*[14] predicted that hydrodynamic phonon transport might appear in suspended graphene at relatively higher temperatures than in bulk materials. Hu *et al.*[15] observed thermal rectification in graphene nanoribbons (GNRs) and claimed the importance of controlling heat flow in graphene nanostructures. Much effort is also devoted to explicate the role of vacancy defects, isotope doping, chemical functionalization, and other factors in tuning the thermal properties of graphene,[16–19] which paves the way for the design of energy-efficient microelectronics. Chen *et al.*[5] experimentally found that isotopically purified graphene has higher thermal conductivity than natural graphene. Kim and Grossman[18] revealed that the graphene superlattice functionalized with hydrogen and pentane has large reduction in thermal conductivity and small reduction in electrical conductivity, which is potential for thermoelectric applications. Cao *et al.*[19] proposed designing networked nanoconstrictions to control heat flux in graphene, which could tune the thermal transport property of graphene by as much as 96%.

Excellent experimental studies[1–4] have been conducted to measure the thermal conductivity of graphene, but the measured values strongly rely on a variety of factors including sample quality, sample size, experimental strategy, and measurement temperature. Especially for Raman techniques, improper choice of laser absorption rate might substantially affect the accuracy of measured thermal conductivity.[8] Numerically solving the linearized Boltzmann transport equation (BTE)[20,21] is one way to compute the thermal properties of graphene, however, only three-phonon processes are considered in this method. Without counting the scattering rates of four-phonon and higher-order processes, the BTE predictions may overestimate the phonon relaxation time as well as the thermal conductivity for graphene.[22] Due to the great challenges in experimental measurements and BTE analyses, the molecular dynamics (MD) simulations, including all the anharmonic interactions, are of great importance to illuminate the thermal properties of graphene. Zhong *et al.*[23] found that the thermal conductivity of few-layer graphene depends on the temperature, the chirality, and the number of atomic planes using nonequilibrium MD (NEMD) method. Zhang *et al.*[24,25] studied the effects of vacancy defects and isotope scattering on graphene thermal conductivity based on the equilibrium MD (EMD). Yao and Cao[26] observed the phenomenon of thermal wave propagation in graphene by NEMD simulations. Ong and Pop[27] investigated the thermal transport of supported graphene with the aid of both EMD and NEMD simulations. The thermal properties of graphene-based materials such as GNRs,[28] graphene nanomesh,[29] and graphene oxide[30] can also be obtained from MD simulations.

[a)]Author to whom correspondence should be addressed. Electronic mail: caoby@tsinghua.edu.cn. Tel./Fax: +86-10-6279-4531.

Empirical potentials describing the atomic interactions play an extremely significant role in MD simulations. The most commonly used potentials for graphene include the Tersoff,[31,32] Tersoff-2010,[33] REBO,[34,35] and AIREBO[36] potentials. The Tersoff-2010 potential is developed by reparameterization[33] on the base of the original Tersoff potential, and is optimized to display better dispersion curves for graphene. The AIREBO potential is an extension of the REBO potential, which includes covalent bonding (REBO) interactions, torsion interactions and Lennard-Jones potential.[36] However, as shown in Table I, significant discrepancies exist in the calculated values of graphene thermal conductivity[24,27,28,37–42] due to the choice of potential, method, and in-plane size. Evans *et al.*[38] reported the highest thermal conductivity for graphene, which is one or two orders of magnitude larger than other computation results. It should be noted that the substantially different value given by Ref. 38 might be due to the unique choice of heat current formula, because various heat current calculations may give significantly different results when using the Green-Kubo method.[43,44] However, the comparison of heat current formulas is beyond the scope of this paper. It was found that the original Tersoff estimates 66% lower value of thermal conductivity than the Tersoff-2010.[37] The thermal conductivity given by the Tersoff-2010 is about 1000-2000 W/(m K), and the calculated values seem to decrease with increasing system size.[37,39,40] Similar trend has also been observed when applying the Green-Kubo method to diamond[45] and silicon[46] in EMD simulations. When the simulation domain is very small, limited phonons are presented to satisfy three-phonon scattering processes, and may pass the system several times without boundary scattering because of periodic boundary conditions. Thus, artificial high thermal conductivity is given by the Green-Kubo formula owing to the memory effects.[45] Therefore, it should be affirmed that size effects have been eliminated when using the Green-Kubo method in EMD simulations. Based on the REBO potential, Ref. 24 reported a higher value for graphene thermal conductivity than Ref. 27. As size effects are not negligible when system size is relatively small,[46] Ref. 24 might overestimate the thermal conductivity for graphene. Considering the thermal conductivity of armchair GNR, the AIREBO potential gives a low value of only 54 W/(m K),[41] one quarter of the value given by the Tersoff potential.[28] Because of the quantum correction used in Ref. 42, the calculated value of Ref. 42 is much higher than Ref. 41. Due to the fact that the method and system size are usually inconsistent in Refs. 24, 27, 28, and 37–42, it is of great difficulty to investigate the performance of the commonly used potentials. Therefore, it is necessary to compare the potentials with the same method and system size.

Since phonons are the main energy carriers in graphene for heat transport, it is important to analyze the effects of potentials on phonon properties. Lindsay and Broido[33] employed the original Tersoff, Tersoff-2010, and REBO potentials to calculate the dispersion curves of graphene using the BTE. It was found that the Tersoff-2010 presents a much better description than the original Tersoff, and gives the most accurate Γ point velocities for in-plane acoustic modes compared with experimental values.[33] Koukaras *et al.*[47] examined the temperature dependence of the G peak using the Tersoff-2010 and AIREBO potentials and found that only the Tersoff-2010 potential exhibits the most suitable behavior in agreement with experimental data. Khan *et al.*[48] studied the thermal conductivity of GNRs using the Tersoff-2010 and REBO potentials in EMD simulations, and it showed that the Tersoff-2010 demonstrates to be a more appropriate model of computing the thermal conductivity as well as describing the phonon transport in GNRs. Phonon relaxation time is also one of the most essential physical properties for graphene, which is often utilized to estimate the lattice thermal conductivity contributed from each mode.[37,49] To calculate the phonon relaxation time of graphene, Ref. 50 used the original Tersoff while Ref. 51 utilized the Tersoff-2010, and the former reported generally higher values than the latter. Despite the previous work on graphene phonon properties, the effects of potentials have not been fully understood.

In this paper, we use EMD simulations to investigate the effects of potentials on the phonon properties of graphene based on the lattice dynamics theory. In Sec. II, we describe the methods and simulation details. Next, we present the results of the phonon dispersion, phonon density of states (PDOS), group velocities, phonon relaxation time, and the

TABLE I. Thermal conductivity of graphene and GNR derived from MD simulations.

Sample	λ [W/(m K)][a]	Potential	Method	System size
GNR[28]	218	Tersoff	NEMD	11 nm × 2 nm, armchair
Graphene[37]	541	Tersoff	EMD	6 nm × 6 nm
Graphene[38]	10 000	Tersoff	EMD	15 nm × 15 nm
Graphene[37]	1 606	Tersoff-2010	EMD	6 nm × 6 nm
Graphene[39]	1 100	Tersoff-2010	EMD	10 nm × 10 nm
Graphene[40]	1 015	Tersoff-2010	EMD	21 nm × 21 nm
Graphene[24]	815	REBO	EMD	5 nm × 5 nm
Graphene[27]	256	REBO	EMD and NEMD	30 nm × 5 nm
GNR[41]	54	AIREBO	NEMD	10 nm × 2 nm, armchair
GNR[42]	272	AIREBO	NEMD[b]	11 nm × 2 nm, armchair

[a]Thermal conductivity at room temperature.
[b]Quantum correction is applied for system temperature.

thermal conductivity of graphene using the original Tersoff, Tersoff-2010, REBO, and AIREBO potentials. Furthermore, we compare the calculation results with experimental data to assess the performance of the potentials. At the end, appropriate conclusions are provided to illustrate the effects of different potentials on the phonon properties of graphene.

II. METHODS AND SIMULATION DETAILS

A. Potential models

1. Tersoff model

The Tersoff model describes the atomic interaction V_{ij} as follows:

$$V_{ij} = f_{ij}^C\left(f_{ij}^R - b_{ij}f_{ij}^A\right), \tag{1}$$

$$f_{ij}^R = Ae^{-\lambda_1 r_{ij}}, \tag{2}$$

$$f_{ij}^A = Be^{-\lambda_2 r_{ij}}, \tag{3}$$

where r_{ij} is the distance between atoms i and j. f_{ij}^C represents the truncation function that limits the interaction within the nearest neighbors. f_{ij}^R and f_{ij}^A stand for attractive and repulsive terms, respectively. b_{ij} is the many-body term, which depends on the bond angle and local coordination of atoms around atom i. The corresponding parameters for the original Tersoff potential are provided in Ref. 32, and the optimized ones for the Tersoff-2010 potential are listed in Ref. 33.

2. REBO model

The REBO model is written as

$$V_{ij} = f_{ij}^C\left(f_{ij}^R - \bar{b}_{ij}f_{ij}^A\right), \tag{4}$$

$$f_{ij}^R = \left(1 + \frac{Q}{r_{ij}}\right)Ae^{-\alpha r_{ij}}, \tag{5}$$

$$f_{ij}^A = \sum_{n=1}^{3} B_n e^{-\lambda_n r_{ij}}, \tag{6}$$

where a few terms have similar meanings to the Tersoff model. $\bar{b}_{ij}$ is the many-body term including the dihedral bending function. The REBO model has more exponential terms compared to the Tersoff model, and the detailed parameters can be found in Ref. 35.

3. AIREBO model

The AIREBO model is developed from the REBO model with an additional LJ term and torsion term

$$V_{ij} = V_{ij}^{REBO} + V_{ij}^{LJ} + \sum_{k\neq i,j}\sum_{l\neq i,j,k} V_{ij}^{TORSION}, \tag{7}$$

$$V_{ij}^{LJ} = 4\varepsilon\left[\left(\frac{\sigma}{r_{ij}}\right)^{12} - \left(\frac{\sigma}{r_{ij}}\right)^{6}\right], r_{ij} < r_c, \tag{8}$$

where ε is the energy parameter, σ is the distance parameter, and r_c is the cutoff distance. All the parameters are provided in Ref. 36.

B. Calculation methods

1. Green's function method

The dispersion curves of graphene can be generated from the Green's function method.[52,53] The equilibrium positions of lth unit cell are defined as $\mathbf{r}_l$ and the position of kth basis atom in the cell is $\mathbf{r}_{lk}$. Due to the lattice vibrations at finite temperature, the atoms are displaced from $\mathbf{r}_{lk}$ by an amount of $\mathbf{u}_{lk}$. The displacement in the reciprocal space is obtained from the Fourier transformation of the real space ones[53,54]

$$\tilde{\mathbf{u}}_{k\alpha}(\mathbf{q}) = \frac{1}{\sqrt{N_T}}\sum_l \mathbf{u}_{lk\alpha}\exp\left(-i\mathbf{q}\cdot\mathbf{r}_l\right). \tag{9}$$

Here α is the direction in Cartesian coordinates, $\mathbf{q}$ is the wave vector, and N_T is the total number of unit cells. The Green's function in reciprocal space is defined as

$$\tilde{\mathbf{G}}_{k\alpha,k'\beta}(\mathbf{q}) = \left\langle\tilde{\mathbf{u}}_{k\alpha}(\mathbf{q})\,\tilde{\mathbf{u}}^*_{k'\beta}(\mathbf{q})\right\rangle, \tag{10}$$

where * means the complex conjugate and $\langle\cdots\rangle$ denotes the ensemble average. With the Green's function method, the dynamical matrix can be described as

$$\mathbf{D}_{k\alpha,k'\beta}(\mathbf{q}) = \frac{k_BT}{m_c}\left[\tilde{\mathbf{G}}^{-1}(\mathbf{q})\right]_{k\alpha,k'\beta}, \tag{11}$$

where m_c is the mass of carbon atom, k_B is Boltzmann's constant, and T is the temperature. By solving the eigenvalues of $\mathbf{D}$, we can get the frequencies of all phonon modes,

$$4\pi^2\nu^2 e_{k\alpha} = \sum_{k',\beta} D_{k\alpha,k'\beta}e_{k'\beta}, \tag{12}$$

where ν is the phonon frequency and $\mathbf{e}$ is the polarization vector. Hence, the relations between $\mathbf{q}$ and ν are obtained. The PDOS curve is computed from the phonon dispersion by dividing the frequency range into many small segments and counting the number of states in each segment. The group velocities are generated from

$$v_g = 2\pi\frac{\partial\nu}{\partial q}. \tag{13}$$

2. Spectral energy density (SED)

The phonon relaxation time of graphene can be calculated by the SED analyses.[55] The SED represents the average kinetic energy per unit cell, which is computed from

$$\Phi(\mathbf{q},\nu)=\frac{m_c}{4\pi N_T\tau_0}\sum_{\alpha}\sum_{k=0}^{1}\left|\int_0^{\tau_0}\sum_{l}^{N_T}\dot{u}_\alpha(l,k,t)\times\exp\left(\mathrm{i}\mathbf{q}\cdot\mathbf{r}_l-2\pi i\nu t\right)\right|^2 dt, \tag{14}$$

where $\dot{u}_\alpha$ is the atom velocity in the α direction, t is the time, and τ_0 is the total integration time. Polarization vectors are demonstrated to be unnecessary in SED analyses[56] and so do not appear in Eq. (14). The phonon relaxation time is obtained by fitting each SED peak to the Lorentzian function as

$$\Phi_s(\mathbf{q},\nu)=\frac{I_s}{1+\left[2\left(\nu-\nu_c\right)/\gamma\right]^2}, \tag{15}$$

$$\tau=1/\gamma, \tag{16}$$

where I_s is the peak magnitude of the s branch, ν_c is the peak center frequency, and γ is the width at half-maximum.

3. Green-Kubo method

The thermal conductivity of graphene is derived from the Green-Kubo method[57] as the finite size and boundary effects are much smaller in EMD simulations compared with NEMD simulations. The Green-Kubo method has been widely used to compute the thermal properties,[27,38,39] which is expressed as

$$\lambda_{\alpha\alpha}=\frac{1}{Vk_BT^2}\int_0^{\tau_m}\langle J_\alpha(0)J_\alpha(t)\rangle\,dt, \tag{17}$$

where V is the system volume, $J_\alpha(t)$ is the α component of the heat current flux at t moment, and $\lambda_{\alpha\alpha}$ is the thermal conductivity along α coordinate. The in-plane thermal conductivity of graphene is the average of $\lambda_{\alpha\alpha}$ and $\lambda_{\beta\beta}$.

C. Simulation details

The computational system contains 20×20 unit cells and periodic boundary conditions are employed in the in-plane directions. The time step is 0.5 fs. Firstly, the system is set up to 300 K by the NVT (constant mass, volume, and temperature) ensemble with the Nosé-Hoover thermostat[58] for 1 ns. Then, it evolves in the NVE (constant mass, volume, and energy) ensemble for the next 3 ns to eliminate the influence of removing the thermostat. At last, the system is run in the NVE ensemble for 1 ns to record the atomic displacements and atomic velocities. With the aid of the PHONON_PACKAGE proposed by Kong,[53] the phonon dispersion can be directly obtained from the atomic displacements. The atomic velocities extracted from the MD simulations are utilized to compute the phonon relaxation time based on the SED. We find that it is sufficient to obtain reliable phonon relaxation time values when the total integration time is beyond 200 ps.

The EMD simulations are also applied to calculate the thermal conductivity of graphene at a temperature of 300 K. The computational system is a 19.7 nm × 20.4 nm graphene sheet with periodic boundary conditions in the in-plane directions. The thickness of the graphene sheet is set as 0.335 nm. We have evaluated that the finite size and boundary effects are negligible after the system domain is larger than 14.8 nm × 15.3 nm. It should be noted that size effects could be ignorable when system length is in nanoscale within the framework of EMD simulations, however, may be noticeable for other methods when computing the thermal conductivity of graphene. The solutions of BTE[20,59,60] have uncovered that the thermal conductivity continues to increase with the increasing size when the characteristic length is on micron order or even millimeter level, owing to long mean free path of long-wavelength phonons in graphene.[61] The autocorrelation length is set as 100 ps, which is long enough to obtain the converged heat current auto-correlation. All the simulations are implemented by the LAMMPS package,[62] and 15 independent runs are performed and averaged for each case study to minimize the influence of statistical fluctuations.

III. RESULTS AND DISCUSSIONS

A. Phonon dispersion curves

Figure 1 presents the dispersion curves of graphene derived from the Tersoff, Tersoff-2010, REBO, and AIREBO potentials by Green's function method. The dispersion curves derived from the Tersoff and Tersoff-2010 potentials have excellent agreement with Ref. 33, validating the accuracy of Green's function method. As can be seen in Fig. 1, all the potentials used here can produce a good description of certain phonon modes, but the calculated curves have some discrepancies with the experimental values.[63,64]

As shown in Figs. 1(a) and 1(b), the original Tersoff potential properly describes the ZO branch while Tersoff-2010 overestimates the ZO phonon frequencies. In addition, the Tersoff potential fails dramatically on the in-plane optical modes while Tersoff-2010 gives a significant improvement of the TO and LO branches. Especially at the Γ point, the TO and LO phonon frequencies derived from the Tersoff potential are about 67 THz, nearly 43% higher than that from experiments. Despite a good description of the LA branch, the Tersoff potential dramatically overestimates the TA branch and underestimates the ZA branch. Especially around the K point, the TA frequencies given by the Tersoff are about 23 THz higher than the experimental values. The Tersoff-2010 generally gives a good description of all the acoustic modes as compared with the experimental dispersion.

As seen in Figs. 1(c) and 1(d), the AIREBO and REBO potentials give similar dispersion curves except the ZA and ZO branches. For the M-K zone, the ZA branch is accurately described by the REBO potential, while the ZA branch derived from the AIREBO undershoots the data by as much as 4 THz. The REBO and AIREBO potentials both fail to describe the ZA phonons near the Γ point. The AIREBO potential dramatically underestimates the ZO branch while the REBO somewhat overestimates the ZO branch. Particularly for the

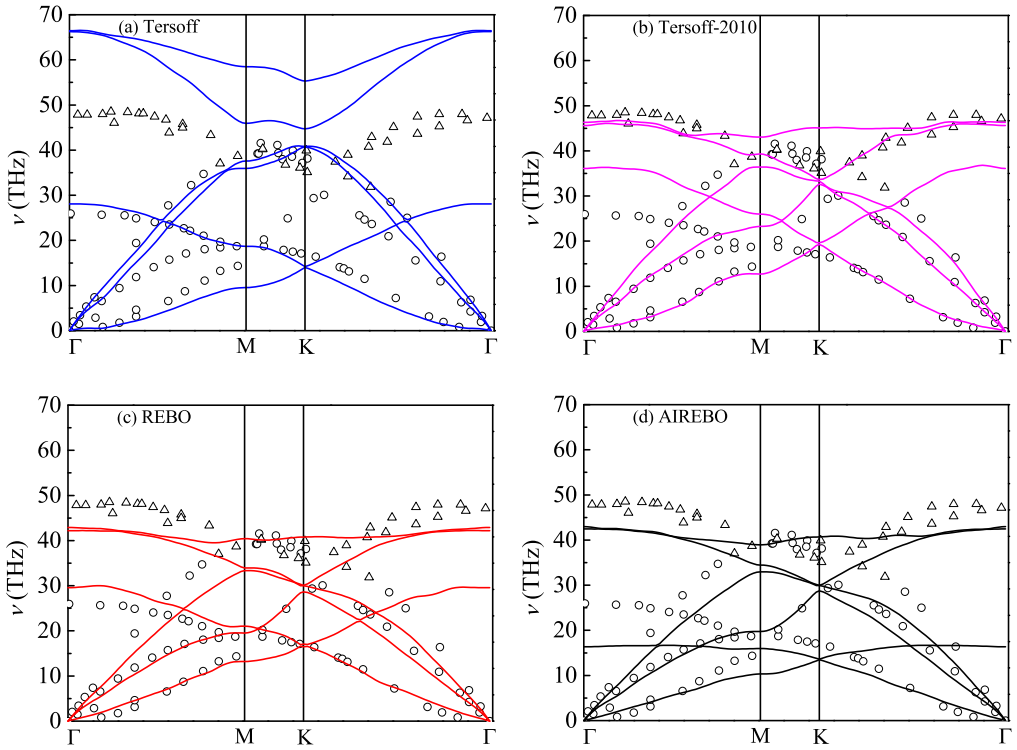

FIG. 1. Phonon dispersion of graphene calculated by (a) Tersoff, (b) Tersoff-2010, (c) REBO, and (d) AIREBO potentials at 300 K. Γ, M, and K are high-symmetry points in the first Brillouin zone. Triangles and circles are in-plane experimental data for graphite from Refs. 63 and 64, respectively.

ZO phonon at Γ point, the frequency values given by the REBO and the AIREBO are about 20% higher and 36% lower in comparison with the experimental data, respectively. Both of the REBO and AIREBO potentials underestimate the LA, TO, and LO branches while the description of the TA branch agrees well with the experimental dispersion.

In comparison with the experimental data, the Tersoff best produces the LA and ZO branches while the Tersoff-2010 best describes the ZA and TO branches. Furthermore, the REBO (or AIREBO) provides the most accurate TA branch. In addition, the Tersoff and Tersoff-2010 potentials properly describe the quadratic dispersion[20,33] of the ZA branch while the REBO and AIREBO potentials give a nearly linear relation for the ZA modes. In summary, the Tersoff-2010 and the REBO potentials generally give the best description of dispersion curves for graphene among the used potentials.

B. Phonon density of states (PDOS)

The G peak is an important signature of graphene PDOS, and the temperature dependence of the G peak can be available to detect the local temperature rise in the Raman spectrum experiment.[1–4,65,66] The Raman G peak frequency is about 47 THz for graphene at 300 K.[1] As shown in Fig. 2, the Tersoff potential is unable to display a clear G peak and gives a peak of 60 THz in the high-frequency region. The G peak frequency obtained from the Tersoff-2010 is around

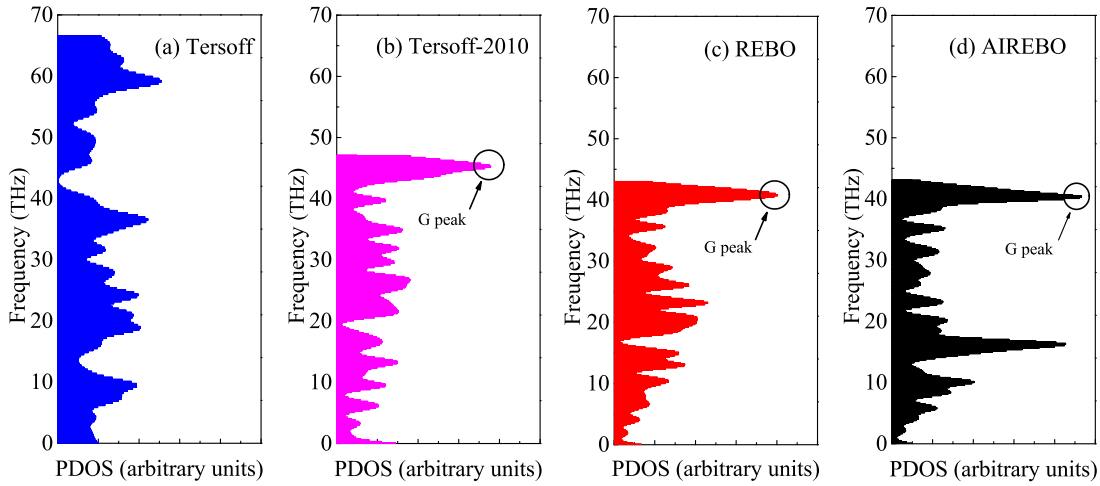

FIG. 2. PDOS of graphene using (a) Tersoff, (b) Tersoff-2010, (c) REBO, and (d) AIREBO potentials.

46 THz, which is very close to the experimental value given by Balandin *et al.*[1] The REBO and AIREBO potentials provide lower values for the G peak frequency (nearly 41 THz). Compared with the PDOS given by the REBO potential, the AIREBO provides an extra peak at 17 THz for the graphene PDOS due to large contribution of the ZO modes. What is more, the PDOS derived from the Tersoff-2010 generally has good agreement with the *ab initio* calculation results,[67] which confirms the sound behavior of the Tersoff-2010 potential.

C. Group velocities

Since the acoustic phonons play a major role in the heat conduction,[8,20] we only display the Γ-K group velocities of acoustic branches in Fig. 3. As indicated in Fig. 3, the Tersoff potential gives the highest LA and TA phonon velocities than the other three potentials. Due to the quadratic dispersion, the ZA phonon velocities given by the Tersoff are close to zero around the Γ point, and the Tersoff-2010 also provides a small value of about 1.3 km/s for the zone-center ZA phonon velocity. The ZA phonon velocities calculated by the Tersoff-2010 have a maximum of 8.1 km/s while the highest ZA phonon velocity for the Tersoff is 6.8 km/s. The ZA phonon velocities derived from the AIREBO potential are 4.7 km/s in a wide range of the first Brillouin zone, which are slightly lower in comparison with the REBO potential. The REBO and AIREBO potentials present similar results for the in-plane acoustic phonon velocities. LA and TA phonon velocities at the Γ point are presented in Table II, and the performance of the employed potentials is evaluated with the experimental data.[64] For the Tersoff potential, the calculated LA and TA phonon velocities are 7.3% and 20.8% higher than the experimental values, respectively. The REBO and AIREBO potentials slightly underestimate the in-plane acoustic phonon velocities at the Γ point. The Tersoff-2010 provides the most accurate LA and TA phonon velocities at the zone-center and the discrepancies are within 2.3% compared with the experimental data.

D. Phonon relaxation time

In Fig. 4, we present the SED along the Γ-K direction at $q = q_{max}/2$ using the Tersoff-2010 potential as a test case. The resolution of the frequency axis is 0.01 THz, which is small enough to catch the SED peak accurately. As shown in Fig. 4, six peaks correspond to six phonon modes and the phonon relaxation times are obtained by fitting each peak to the Lorentzian function. Similar peak-and-valley plots can also be observed along the entire frequency range at the other allowed wave vectors. It should be noted that the locations of the peaks in the SED are in excellent agreement with the phonon frequencies derived from the Green's function method, which confirms the self-consistency of our methods. Based on the SED analyses, we use the Tersoff, Tersoff-2010, REBO, and AIREBO potentials to compute the phonon relaxation times. Fig. 5 presents the frequency-dependent relaxation times of graphene at room temperature on a logarithmic scale. As indicated in Figs. 5(a)-5(d), the Tersoff-2010 gives the highest values of relaxation time for low-frequency (<5 THz)

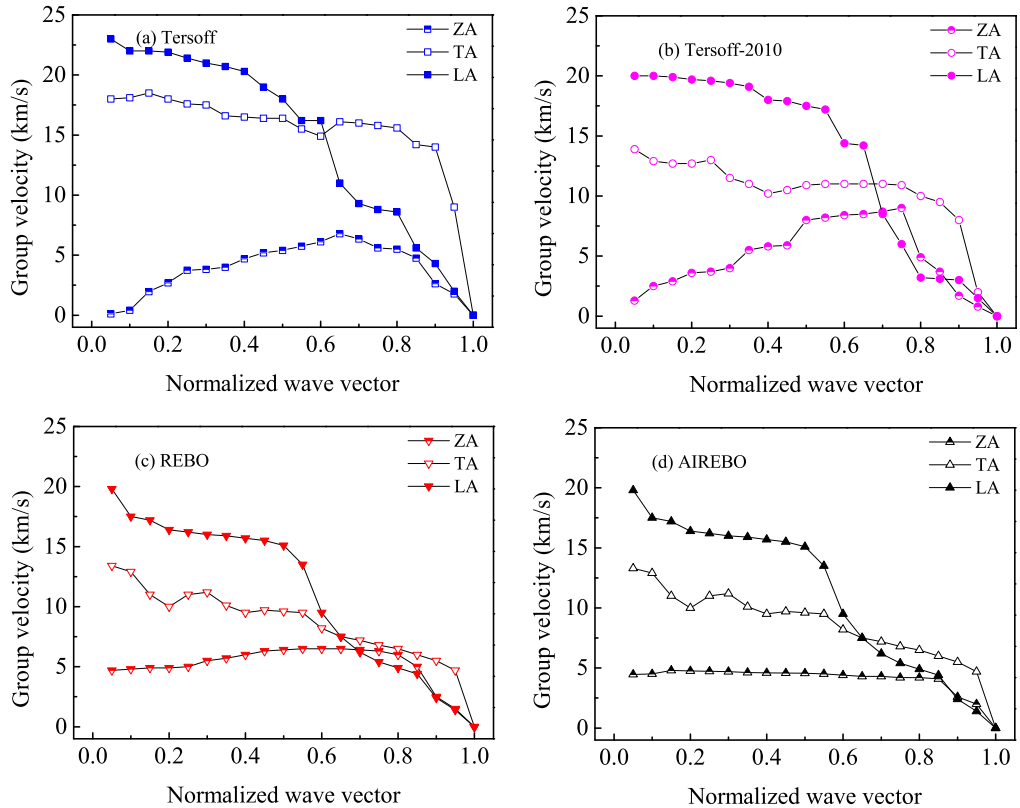

FIG. 3. Group velocities of graphene using (a) Tersoff, (b) Tersoff-2010, (c) REBO, and (d) AIREBO potentials. Normalized wave vector denotes the direction from Γ to K.

TABLE II. Phonon thermal properties of graphene from different potentials.

Properties	Tersoff	Tersoff-2010	REBO	AIREBO	Experiment
Best dispersion branches[a]	LA and ZO	ZA and TO	TA	TA	...
v_{LA} (km/s)[b]	23.4	21.3	20.3	20.1	21.8[c]
v_{TA} (km/s)[b]	18.0	14.7	13.4	13.3	14.9[c]
G peak frequency (THz)	...	46	41	41	47[d]
τ_{LA}[e]	Poor	Most close	Poor	Poor	...
τ_{TA}[e]	Poor	Most close	Poor	Poor	...
λ [W/(m K)][f]	560	1192	275	290	1000-5000[g]
Contribution of TA (%)	37.3	25.7	27.6	28.6	...
Contribution of LA (%)	51.4	44.0	61.4	66.5	...
Contribution of ZA and ZO (%)	10.7	30.0	10.3	<5	...

[a]Compared with Refs. 63 and 64.
[b]Zero-center group velocities.
[c]Reference 64.
[d]Reference 1.
[e]Frequency-dependent relaxation time compared with the ideal curve "$\tau^{-1} \propto \nu^2$."
[f]Thermal conductivity at 300 K derived from the Green-Kubo method.
[g]References 1–7.

acoustic phonons. As seen in Figs. 5(a) and 5(b), the ZO relaxation time values given by the Tersoff-2010 is in a range of 15-20 ps, slightly higher than that given by the Tersoff. Compared with the Tersoff, the Tersoff-2010 estimates higher relaxation time values for the ZA branch, and provides lower relaxation time values for the TA and LA phonons with a frequency larger than 10 THz. As indicated in Figs. 5(c) and 5(d), the REBO potential presents similar values of phonon relaxation time as compared with the AIREBO potential.

On the basis of Klemens's theory,[68,69] the relaxation time satisfies the following relation with frequencies for acoustic phonons (s denotes LA or TA):

$$\tau_s = \frac{1}{4\pi\gamma_s^2}\frac{m_c\bar{v}_{g,s}^2}{k_BT}\frac{\nu_{m,s}}{\nu_s^2}, \tag{18}$$

where γ_s means the Grüneisen parameter, $\bar{v}_{g,s}$ is the average group velocity, and $\nu_{m,s}$ represents the maximum frequency for the s branch. Therefore, the ideal curve "$\tau^{-1} \propto \nu^2$" is added in Fig. 5 to evaluate the actual trends derived from the used potentials. It is found that the relaxation time values given by the Tersoff-2010 are in line with the ideal curve for all acoustic phonons, while the deviation is obvious for the Tersoff. As for the REBO or AIREBO potential, the TA and LA branches deviate most from the ideal curve.

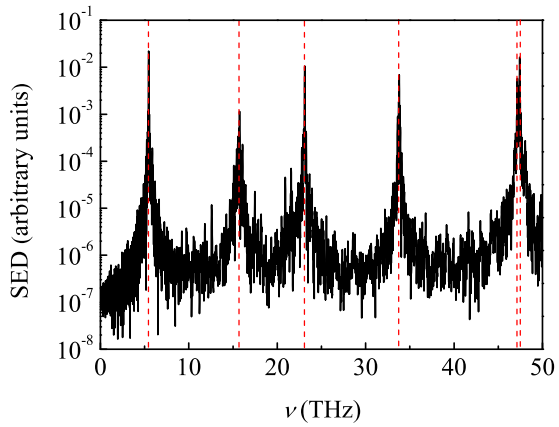

FIG. 4. Semilogarithmic plot of the SED (the case of Tersoff-2010 potential at $q = q_{max}/2$ along the Γ-K direction). The vertical dashed lines indicate the peak positions corresponding to the mode frequencies.

E. Thermal conductivity

1. Thermal conductivity by the Green-Kubo method

As shown in Fig. 6, the Tersoff-2010 estimates the highest thermal conductivity for graphene among the used potentials, giving a value of about 1192 W/(m K). The calculated value given by the Tersoff-2010 has a small discrepancy of only 8.4% with Ref. 39 and agrees well with Ref. 40 within acceptable error range. The Tersoff provides a thermal conductivity value of 560 W/(m K) for graphene, which has good agreement with the simulation results in Ref. 37. The REBO provides a low value of 275 W/(m K) for graphene thermal conductivity, nearly half of the value given by the Tersoff. It was reported that the REBO usually gives lower thermal conductivity values for carbon materials in comparison with the Tersoff.[27,33,70] The REBO and AIREBO potentials give a similar thermal conductivity value for graphene, which indicates that the additional torsion term and Lennard-Jones interactions do not influence graphene thermal properties significantly. It should be noted that the calculated thermal conductivities are not "intrinsic thermal conductivity" of graphene, even though the size effects have been eliminated in the EMD simulations. All the calculated thermal conductivities of graphene are inconsistently low compared with the measured values,[1–4] hence to some extent, the used potentials fail to model the intrinsic thermal conductivity of graphene in EMD simulations. Since this paper is more focused on accessing the performance of the potentials in the framework of EMD simulations rather than presenting intrinsic thermal conductivity of graphene, it might be concluded that the value given by the Tersoff-2010 seems superior to other potentials. Lindsay and Broido[33] used the Tersoff, Tersoff-2010, and REBO potentials to compute the thermal conductivity of

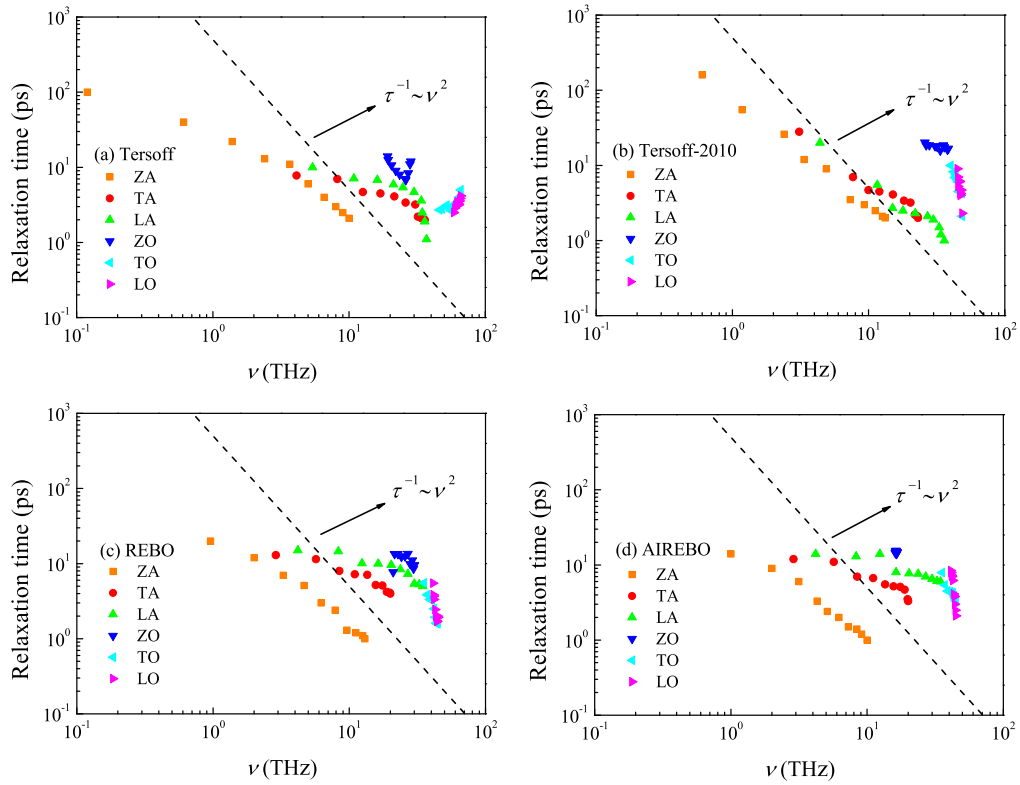

FIG. 5. Frequency-varying relaxation times of graphene using (a) Tersoff, (b) Tersoff-2010, (c) REBO, and (d) AIREBO potentials.

graphene by solving the BTE, and their results showed that the Tersoff-2010 gives a thermal conductivity of 3500 W/(m K) which is most close to measured values while the Tersoff and REBO potentials substantially underestimate this value.

2. Phonon contribution to the thermal conductivity

Based on the BTE with relaxation time approximation (RTA), the thermal conductivity is calculated by

$$\lambda = \sum_s \sum_\nu c_{ph} v_g^2 \tau, \tag{19}$$

where c_{ph} is the phonon specific heat. In classic MD systems, $c_{ph} = k_B/V$ because all phonons are supposed to be excited.

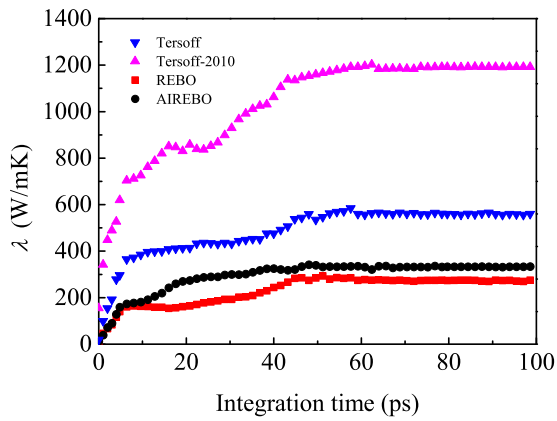

FIG. 6. Thermal conductivity of graphene at 300 K.

It should be noted that phonon Bose-Einstein distribution only exists in a quantum system,[71] the classic definition of specific heat is adopted instead of the quantum definition. Using the group velocities and relaxation times in the Γ-K direction, we can estimate the thermal conductivity contributed from each branch while neglecting the anisotropy of the phonon dispersion.[7] It should be noted that the RTA is widely applied for estimating the mode thermal conductivity in graphene[16,37,49] and CNTs,[55] however, BTE calculations showed that the RTA has a bad performance for graphene.[20] The mode contributions might be roughly computed due to the uncertainty of the RTA. Fig. 7 presents the calculated phonon contribution to the thermal conductivity given by the used potentials. As seen in Fig. 7, the TA and LA branches have a major contribution to graphene thermal conduction for all the potentials, which agrees well with theoretical predictions.[68,69] Based on the SED and BTE with RTA, Refs. 37 and 50 also reported that the in-plane acoustic phonons have a dominant contribution to the thermal conductivity of graphene. The TO and LO phonons are trivial for the thermal conductivity of graphene due to their small group velocities and low relaxation times regarding the calculation results of all the used potentials. However, when it comes to GNRs, Ye *et al.*[49] uncovered that high-frequency optical phonons are not negligible for heat conduction. The Tersoff-2010 estimates a contribution of 30.0% in total for flexural phonons. The Tersoff and REBO potentials both estimate nearly 11.0% contribution for flexural phonons, while the AIREBO gives the lowest contribution (<5.0%) for flexural phonons. Therefore, the flexural phonons are not negligible for graphene thermal transport and may play an important role when coupling

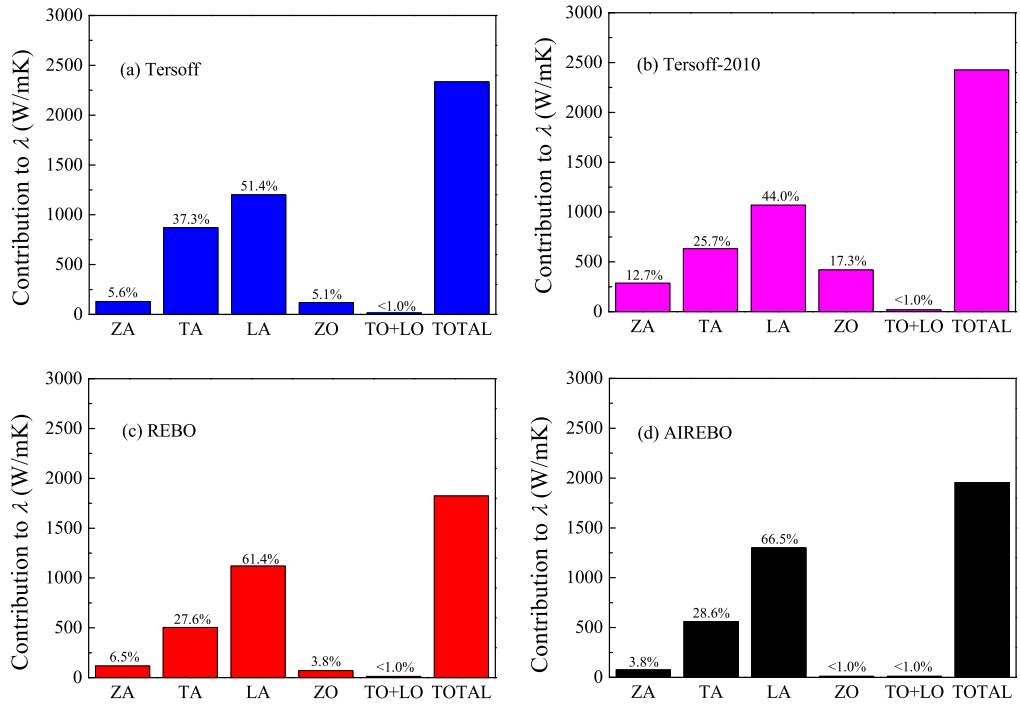

FIG. 7. Phonon contribution to the thermal conductivity derived from (a) Tersoff, (b) Tersoff-2010, (c) REBO, and (d) AIREBO potentials.

with the substrate.[12,20] Qiu and Ruan[51] found that the flexural phonon relaxation times in supported graphene have large reduction due to the breakdown of the selection rule.[20] Due to the overestimation of the phonon specific heat, the calculated total thermal conductivities are higher than the results generated from the Green-Kubo method, but we are more interested in the relative contribution of phonon branches instead of the absolute thermal conductivity values. It should be noted that all phonon modes share the same specific heat, which might overestimate the contributions for LA, TA, and ZO modes while undervaluing the contribution of ZA branch. BTE calculations[20] demonstrated that ZA phonons may dominate the thermal transport in graphene, and one reason is associated with the anomalously large PDOS which results in a large contribution to specific heat for ZA modes.

IV. CONCLUSIONS

In this work, we systematically investigate the phonon thermal properties of graphene using different potentials. The most important results are summarized in Table II. Green's function method is utilized to obtain the dispersion curves of graphene at 300 K. Compared to the experimental data, the original Tersoff best produces the LA and ZO branches while the Tersoff-2010 best describes the ZA and TO branches. In addition, the REBO and AIREBO potentials both provide the most accurate TA branch. The Tersoff-2010 and the REBO potentials exhibit the best overall performance on the phonon dispersion of graphene. As for the G peak frequency of PDOS, the Tersoff-2010 provides the most accurate value (46 THz) compared with Raman spectrum experiment (47 THz). The Tersoff-2010 also correctly calculates the in-plane acoustic velocities at the zone-center while the other potentials perform poorly.

The phonon relaxation time of graphene is obtained from the SED analyses. It is found that the Tersoff-2010 estimates the highest relaxation times for low-frequency acoustic phonons. What is more, the acoustic relaxation time given by the Tersoff-2010 satisfies the ideal curve "$\tau^{-1} \propto \nu^2$" while large deviations are observed for other potentials.

Furthermore, the thermal conductivity of graphene is calculated by the Green-Kubo method. Despite the low values obtained from the MD simulations, the thermal conductivity of graphene given by the Tersoff-2010 is about 1192 W/(m K), which seems superior to other potentials. The REBO potential gives a lower thermal conductivity value for graphene than the Tersoff potential. The REBO and AIREBO potentials provide similar thermal conductivity values for graphene because the additional torsion and Lennard-Jones interactions in the AIREBO have negligible effects. Based on the BTE with RTA, we estimate the contribution of phonon branches to the thermal conductivity. The Tersoff-2010 gives a contribution of 30.0% for flexural phonons, which is higher than the contributions estimated for other potentials.

To summarize, the Tersoff-2010 exhibits the best performance of producing the phonon properties of graphene among the commonly used potentials. Our calculation results provide a comprehensive understanding of the commonly used potentials on calculating the phonon thermal properties of graphene.

ACKNOWLEDGMENTS

This work was financially supported by the National Natural Science Foundation of China (Grant Nos. 51322603, 51676108, 51628602, 51136001, and 51356001), Tsinghua

National Laboratory for Information Science and Technology, and Science Fund for Creative Research Group (Grant No. 51321002).

[1]A. A. Balandin, S. Ghosh, W. Bao, I. Calizo, D. Teweldebrhan, F. Miao, and C. N. Lau, Nano Lett. **8**, 902 (2008).
[2]W. Cai, A. L. Moore, Y. Zhu, X. Li, S. Chen, L. Shi, and R. S. Ruoff, Nano Lett. **10**, 1645 (2010).
[3]L. A. Jauregui, Y. Yue, A. N. Sidorov, J. Hu, Q. Yu, G. Lopez, R. Jalilian, D. K. Benjamin, D. A. Delk, W. Wu, Z. Liu, X. Wang, Z. Jiang, X. Ruan, J. Bao, S. S. Pei, and Y. P. Chen, ECS Trans. **28**, 73 (2010).
[4]S. Ghosh, W. Bao, D. L. Nika, S. Subrina, E. P. Pokatilov, C. N. Lau, and A. A. Balandin, Nat. Mater. **9**, 555 (2010).
[5]S. Chen, Q. Wu, C. Mishra, J. Kang, H. Zhang, K. Cho, W. Cai, A. A. Balandin, and R. S. Ruoff, Nat. Mater. **11**, 203 (2012).
[6]D. L. Nika, E. P. Pokatilov, A. S. Askerov, and A. A. Balandin, Phys. Rev. B **79**, 155413 (2009).
[7]D. L. Nika, S. Ghosh, and E. P. Pokatilov, Appl. Phys. Lett. **94**, 203103 (2009).
[8]A. A. Balandin, Nat. Mater. **10**, 569 (2011).
[9]E. Pop, V. Varshney, and A. K. Roy, MRS Bull. **37**, 1273 (2012).
[10]K. M. F. Shahil and A. A. Balandin, Solid State Commun. **152**, 1331 (2012).
[11]J. D. Renteria, D. L. Nika, and A. A. Balandin, Appl. Sci. **4**, 525 (2014).
[12]J. H. Seol, I. Jo, A. L. Moore, L. Lindsay, Z. H. Aitken, M. T. Pettes, X. S. Li, Z. Yao, R. Huang, D. Broido, N. Mingo, R. S. Ruoff, and L. Shi, Science **328**, 213 (2010).
[13]S. Lee, D. Broido, K. Esfarjani, and G. Chen, Nat. Commun. **6**, 6290 (2015).
[14]A. Cepellotti, G. Fugallo, L. Paulatto, M. Lazzeri, F. Mauri, and N. Marzari, Nat. Commun. **6**, 3 (2015).
[15]J. Hu, X. Ruan, and Y. P. Chen, Nano Lett. **9**, 2730 (2009).
[16]T. Feng, X. Ruan, Z. Ye, and B. Cao, Phys. Rev. B **91**, 224301 (2015).
[17]D. L. Nika and A. A. Balandin, J. Phys.: Condens. Matter **24**, 233203 (2012).
[18]J. Y. Kim and J. C. Grossman, Nano Lett. **15**, 2830 (2015).
[19]B. Cao, W. Yao, and Z. Ye, Carbon **96**, 711 (2016).
[20]L. Lindsay, D. A. Broido, and N. Mingo, Phys. Rev. B **82**, 115427 (2010).
[21]Y. Kuang, L. Lindsay, and B. Huang, Nano Lett. **15**, 6121 (2015).
[22]T. Feng and X. Ruan, Phys. Rev. B **93**, 045202 (2016).
[23]W. R. Zhong, M. P. Zhang, B. Q. Ai, and D. Q. Zheng, Appl. Phys. Lett. **98**, 113107 (2011).
[24]H. Zhang, G. Lee, A. F. Fonseca, T. L. Borders, and K. Cho, J. Nanomater. **2010**, 537657.
[25]H. Zhang, G. Lee, and K. Cho, Phys. Rev. B **84**, 115460 (2011).
[26]W. Yao and B. Cao, Chin. Sci. Bull. **59**, 3495 (2014).
[27]Z. Y. Ong and E. Pop, Phys. Rev. B **81**, 155408 (2010).
[28]Z. Guo, D. Zhang, and X. Gong, Appl. Phys. Lett. **95**, 163103 (2009).
[29]L. Yang, J. Chen, N. Yang, and B. Li, Int. J. Heat Mass Transfer **91**, 428 (2015).
[30]X. Mu, X. Wu, T. Zhang, D. B. Go, and T. Luo, Sci. Rep. **4**, 3909 (2014).
[31]J. Tersoff, Phys. Rev. B **37**, 6991 (1988).
[32]J. Tersoff, Phys. Rev. B **39**, 5566 (1989).
[33]L. Lindsay and D. A. Broido, Phys. Rev. B **81**, 205441 (2010).
[34]D. W. Brenner, Phys. Rev. B **42**, 9458 (1990).
[35]D. W. Brenner, O. A. Shenderova, J. A. Harrison, S. J. Stuart, B. Mi, and S. B. Sinnott, J. Phys.: Condens. Matter **14**, 783 (2002).
[36]S. J. Stuart, A. B. Tutein, and J. A. Harrison, J. Chem. Phys. **112**, 6472 (2000).
[37]L. Chen and S. Kumar, J. Appl. Phys. **112**, 043502 (2012).
[38]W. J. Evans, L. Hu, and P. Keblinski, Appl. Phys. Lett. **96**, 203112 (2010).
[39]T. Feng and X. Ruan, Carbon **101**, 107 (2016).
[40]L. F. C. Pereira and D. Donadio, Phys. Rev. B **87**, 125424 (2013).
[41]T. Y. Ng, J. J. Yeo, and Z. S. Liu, Carbon **50**, 4887 (2012).
[42]B. Zheng, H. Dong, and F. Chen, Acta Phys. Sin. **63**, 076501 (2014).
[43]Z. Fan, L. F. C. Pereira, H.-Q. Wang, J.-C. Zheng, D. Donadio, and A. Harju, Phys. Rev. B **92**, 094301 (2015).
[44]A. Guajardo-Cuellar, D. B. Go, and M. Sen, J. Chem. Phys. **132**, 104111 (2010).
[45]J. Che, T. Cagin, W. Deng, and W. A. Goddard, J. Chem. Phys. **113**, 6888 (2000).
[46]P. K. Schelling, S. R. Phillpot, and P. Keblinski, Phys. Rev. B **65**, 144306 (2002).
[47]E. N. Koukaras, G. Kalosakas, C. Galiotis, and K. Papagelis, Sci. Rep. **5**, 12923 (2015).
[48]A. I. Khan, I. A. Navid, M. Noshin, H. M. Uddin, F. F. Hossain, and S. Subrina, Electronics **4**, 1109 (2015).
[49]Z. Ye, B. Cao, W. Yao, T. Feng, and X. Ruan, Carbon **93**, 915 (2015).
[50]Z. Wei, J. Yang, K. Bi, and Y. Chen, J. Appl. Phys. **116**, 153503 (2014).
[51]B. Qiu and X. Ruan, Appl. Phys. Lett. **100**, 193101 (2012).
[52]C. Campana and M. H. Müser, Phys. Rev. B **74**, 075420 (2006).
[53]L. T. Kong, Comput. Phys. Commun. **182**, 2201 (2011).
[54]L. T. Kong, G. Bartels, C. Campana, C. Denniston, and M. H. Müser, Comput. Phys. Commun. **180**, 1004 (2009).
[55]J. A. Thomas, J. E. Turney, R. M. Iutzi, C. H. Amon, and A. J. H. McGaughey, Phys. Rev. B **81**, 081411 (2010).
[56]T. Feng, B. Qiu, and X. Ruan, J. Appl. Phys. **117**, 195102 (2015).
[57]R. Kubo, J. Phys. Soc. Jpn. **12**, 570 (1957).
[58]W. G. Hoover, Phys. Rev. A **31**, 1695 (1985).
[59]G. Fugallo, A. Cepellotti, L. Paulatto, M. Lazzeri, N. Marzari, and F. Mauri, Nano Lett. **14**, 6109 (2014).
[60]K. S. Mei, L. N. Maurer, Z. Aksamija, and I. Knezevic, J. Appl. Phys. **116**, 164307 (2014).
[61]D. L. Nika, A. S. Askerov, and A. A. Balandin, Nano Lett. **12**, 3238 (2012).
[62]S. Plimpton, J. Comput. Phys. **117**, 1 (1995).
[63]J. Maultzsch, S. Reich, C. Thomsen, H. Requardt, and P. Ordejón, Phys. Rev. Lett. **92**, 075501 (2004).
[64]M. Mohr, J. Maultzsch, E. Dobardžić, S. Reich, I. Milošević, M. Damnjanović, A. Bosak, M. Krisch, and C. Thomsen, Phys. Rev. B **76**, 035439 (2007).
[65]I. Calizo, A. A. Balandin, W. Bao, F. Miao, and C. N. Lau, Nano Lett. **7**, 2645 (2007).
[66]S. Ghosh, I. Calizo, D. Teweldebrhan, E. P. Pokatilov, D. L. Nika, A. A. Balandin, W. Bao, F. Miao, and C. N. Lau, Appl. Phys. Lett. **92**, 151911 (2008).
[67]F. Liu, P. Ming, and J. Li, Phys. Rev. B **76**, 064120 (2007).
[68]P. G. Klemens, J. Wide Bandgap Mater. **7**, 332 (2000).
[69]P. G. Klemens, Int. J. Thermophys. **22**, 265 (2001).
[70]J. Lukes and H. Zhong, J. Heat Transfer **129**, 705 (2007).
[71]J. E. Turney, E. S. Landry, A. J. H. McGaughey, and C. H. Amon, Phys. Rev. B **79**, 064301 (2009).